Supporting Information

Bio-inspired hybrid nanoparticles promote vascularized bone regeneration in a morphology-dependent manner

Gaojie Yang [a,b,‡], Haoming Liu [a,b,‡], Xixi Hu [a,b], Zetao Chen [c,d], Thor E. Friis [d], Jianglin Wang [a,b], Yin Xiao [d,*] and Shengmin Zhang [a,b,*]

[a] Advanced Biomaterials and Tissue Engineering Center, Huazhong University of Science and Technology, Wuhan 430074, China
[b] Department of Biomedical Engineering, Huazhong University of Science and Technology, Wuhan 430074, China
[c] Guanghua School of Stomatology, Hospital of Stomatology, Sun Yat-sen University and Guangdong Provincial Key Laboratory of Stomatology, Guangzhou 510055, People's Republic of China
[d] Institute of Health and Biomedical Innovation & the Australia-China Centre for Tissue Engineering and Regenerative Medicine, Queensland University of Technology, Brisbane 4059, Australia
E-mail addresses: smzhang@hust.edu.cn (S. Zhang), yin.xiao@qut.edu.au (Y. Xiao).
[‡] These authors contributed equally to this work.

Supplemental Section 1: Spatial configuration analysis of the bi-templates

Circular dichroism (CD) quantitative results (inserts) show there are more beta-sheet structures in the system when the second template is introduced, indicating the interactions within the bi-molecular templates. The analysis revealed that the secondary structure of the primary template (collagen) was dominated by random coils. When the second regulating templates (CS, SA, or PAA) were allowed to interact with collagen, the random coils and β-turns partially transformed to β-sheets (Fig. S1).

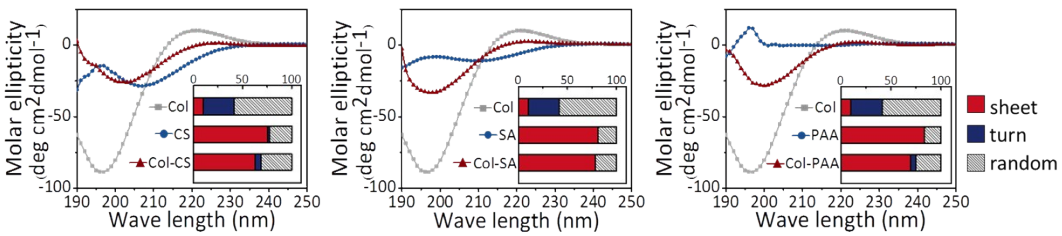

Fig. S1. CD spectra analysis for the secondary structure of the templates.

The increases of the β-sheet content are likely due to the inductive effect of hydrogen bonds within the bi-templates. Because of the periodicity of the pendant carboxyl groups on the main chain of CS, SA and PAA, intramolecular hydrogen bonds are easily formed between collagen and each regulating template, which then changes steric configuration of the resulting binary systems.

Fourier transform infrared spectroscopy (FTIR) analysis of the bi-templates showed the absorption peaks for –C=O and C–N stretching vibrations in amide groups which shifted to low wavenumber regions when the regulating templates were incorporated, a result that confirmed the presence of hydrogen bonds (Fig. S2).

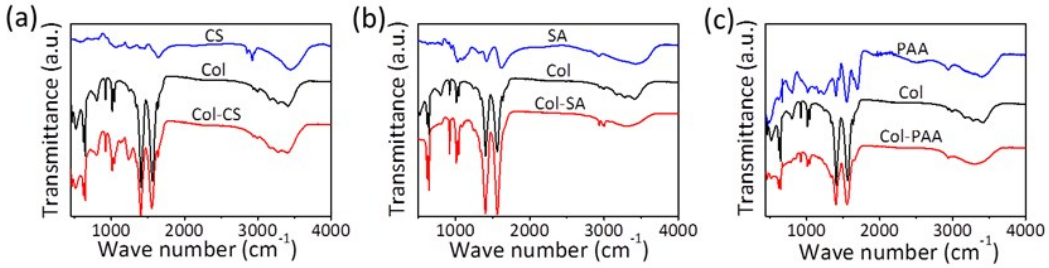

Fig. S2. ATR-IR spectral of CS (a), SA (b), PAA (c) and their respective composite templates with Col.

Supplemental Section 2: Conventional synthesis of nanoparticles in bulk solution

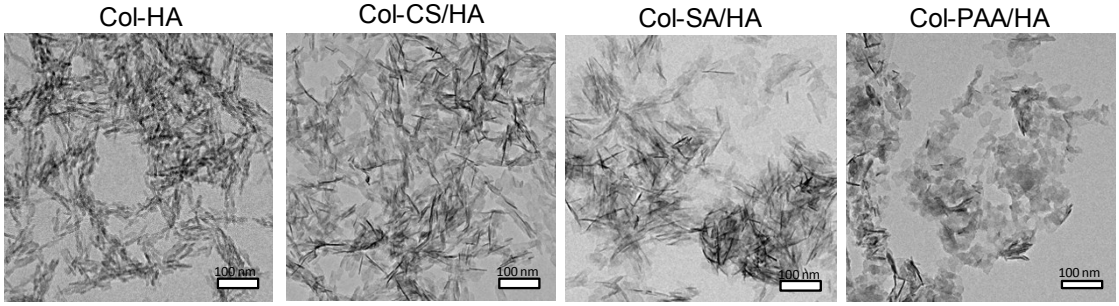

Fig. S3. TEM images of nanoparticles synthesized via conventional wet chemistry. It was observed that only HA nanoplates were obtained using either Col-CS, Col-SA or Col-PAA as the template, due to the fast and uncontrollable precipitation reaction when Ca/P coexisting in solution.

Supplemental Section 3: Physico-chemical characterization of the nanoparticles

Three types of NPs exhibited similar FTIR absorption at approximately 1030 cm^{-1}, which is associated with the characteristic phosphate stretching vibration. Besides, the FTIR spectra all revealed similar absorption peaks at 1667 cm^{-1}, 1551cm^{-1} and 1325 cm^{-1}, which is attributed to amide group of Col in all groups (Fig. S4a). X-ray diffraction (XRD) analysis showed two characteristic peaks for hydroxyapatite: 2θ = 25.9° (002) and 2θ = 32.8° (211) in all NP groups (Fig. S4b).[2] Energy-dispersive X-ray spectrum (EDX) was used for quantitative analysis of the element content of the particles and showed the Ca/P ratio to be approximately 1.6 in all groups (Fig. S4c), which is similar to that of natural bone. It is noteworthy that the Ca/P ratio fell from 1.66 for HANN to 1.61 for HANF and 1.57 for HANF, which supports to the hypothesis that binary-templates significantly affect HA mineralization assemblies by binding with Ca^{2+}.

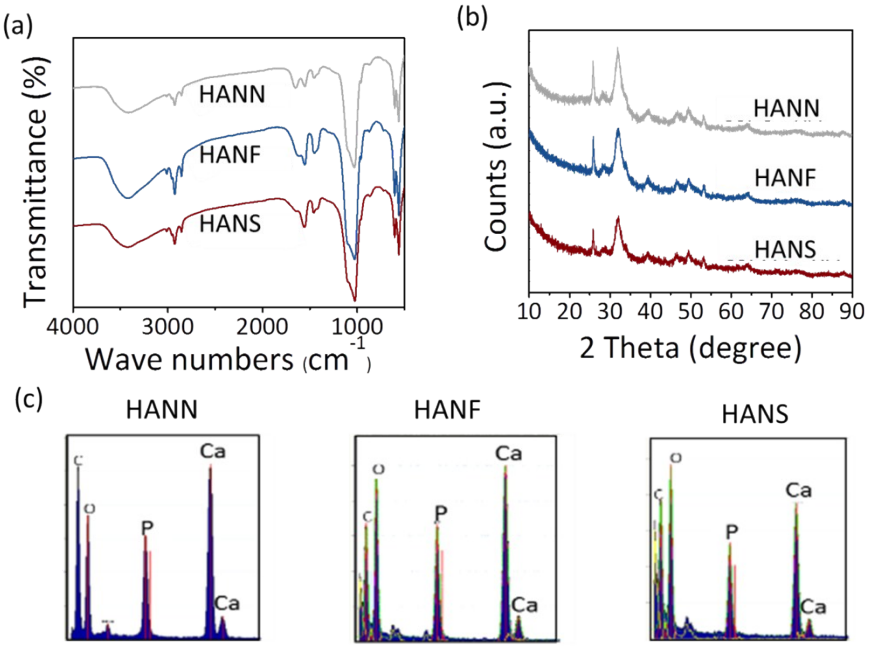

Fig. S4. FT-IR (a), XRD (b), and EDX (c) analysis for the NPs in different groups, which confirmed the inorganic component in the NPs is hydroxyapatite.

Thermo gravimetric analysis (TGA) curves present a notable two step weight loss (Fig. S5a). The first stage corresponds to water evaporation, and the second stage is due to the combustion of organic components. According to the differential thermal analysis (DTA, Fig. S5b-S5d), there were two distinct weight-loss peaks between 250 and 500°C in both HANN and HANF groups, which correspond to the thermal-decomposition of the less stable polysaccharides (CS and SA) and the more stable protein (Col). For the HANS group, there was only one weight-loss plateau between 250-500°C, due to the similar backbone structure for its two organic components (polyamide).

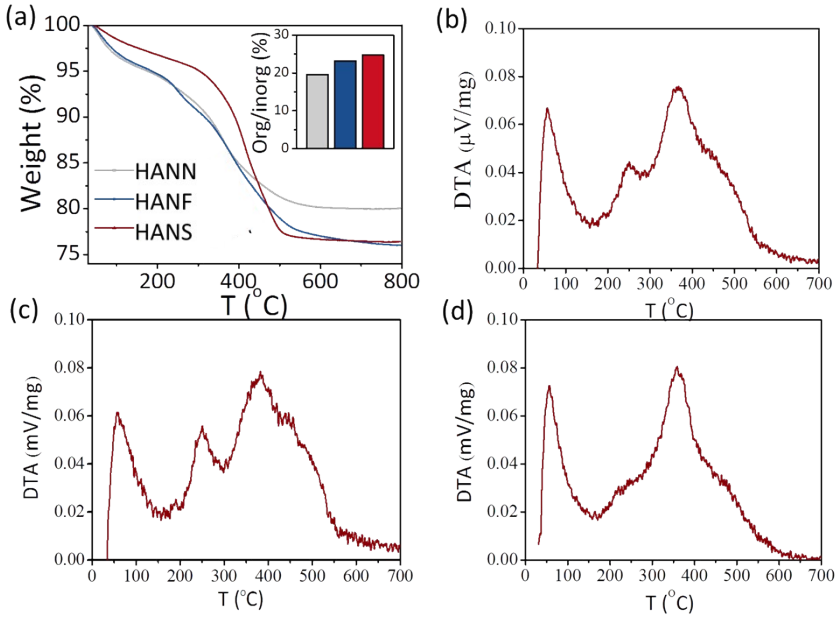

Fig. S5. TG (a) and DTA analysis of HANN (b), HANF (c), HANS (d). Note that two distinct weight-losing peaks between 250-500 °C were evidenced in HANN and HANF group, corresponding to the thermal-decomposition for the less stable polysarccide (CS or SA) between 250-375°C and more stable protein (Col) between 375-500°C, respectively. For Col-PAA/HA group, there is only one weight-losing plateau between 250-500 °C.

Surface zeta potential for HANN, HANF and HANS NPs were +1.74 mV, -2.27 mV and -15.3 mV, respectively (Fig. S6), and the negative surface charge for HANS particles can facilitate the cellular uptake.

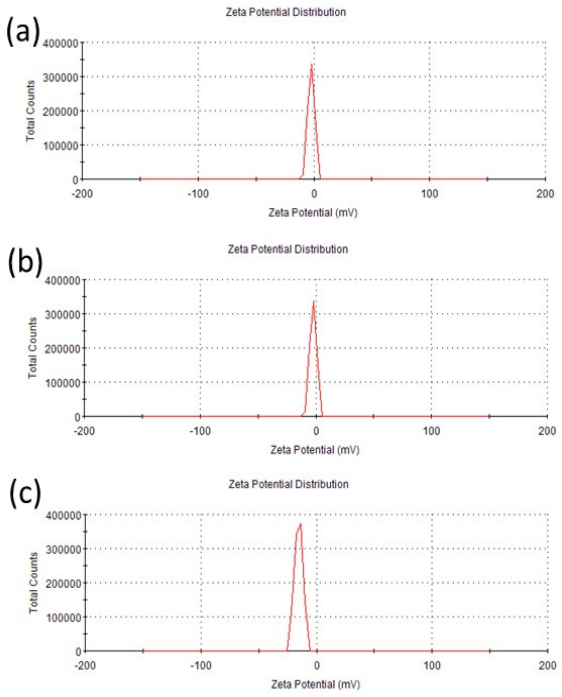

Fig. S6. Surface Zeta potential of HANN (a), HANF (b), HANS (c) in ddH_2O. It was found that Col-PAA/HA NPs had the most negative surface charge (-15.3 mV), while Col-CS/HA was nearly electroneutral (+1.74 mV).

Supplemental Section 4: Morphology characterization of the uni-template nanoparticles

As shown in Fig. S7, Nanorods with different aspect ratio (approximately 200 nm in length) were obtain using Col or CS single template (termed as Col/HA and Col/CS respectively); SA induced the formation of plate-like HA nanoparticles (SA/HA, 100 nm in dimension); Nanospheres were prepared with PAA as the template (PAA/HA, less than 50 nm in diameter). Comparing the the morphology of the bi-templates induced NPs as shown in Fig. 2a&2b, the nanoneedles in HANN group can be seen packed into bundles, and are longer than the corresponding uni-template CS/HA NPs. Using Col-SA as a template resulted in HANF which were similar in length to but wider in shape than its uni-template counterpart (SA/HA). PAA can induce the formation of spherical nano-apatite, a finding that has been documented by earlier studies.[1] Our experiments show that the PAA/HA uni-template NPs were spherical with diameters of less than 50 nm and which assembled into string-like structures when collagen was introduced into the bi-template system.

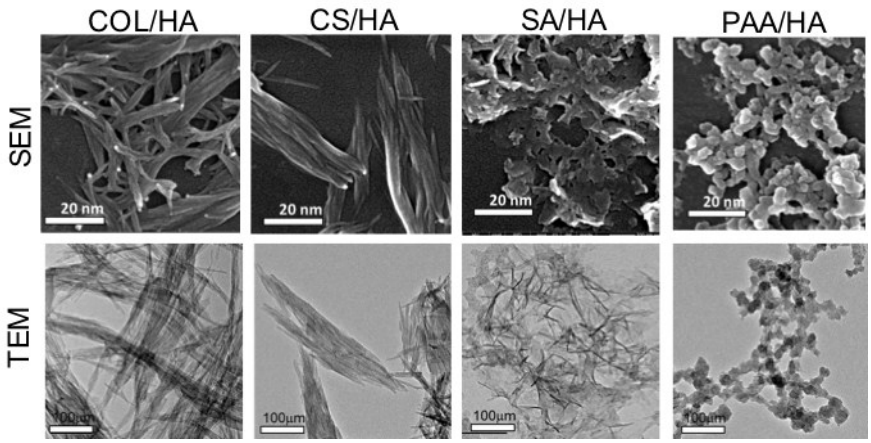

Fig. S7. SEM (upper) and TEM (bottom) micrograph of the uni-template nanoparticles.

Supplemental Section 5: immunofluorescent for osteogenic differentiation

Followed by treatment with NP-contained osteogenic induction medium, the degree of stem cell differentiation was measured by immunofluorescent (IF) staining. IF images show that higher level of osteogenic-related protein were expressed after the NPs treatment (Fig. S8a). Quantification analysis also shows that the fluorescent intensity for all the three markers (OCN, ONN, and OPN) in HANS group was significantly higher than other three group (Fig. S8b, $p < 0.05$). The *in vitro* results support a strong association between autophagy activation and osteogenic differentiation.

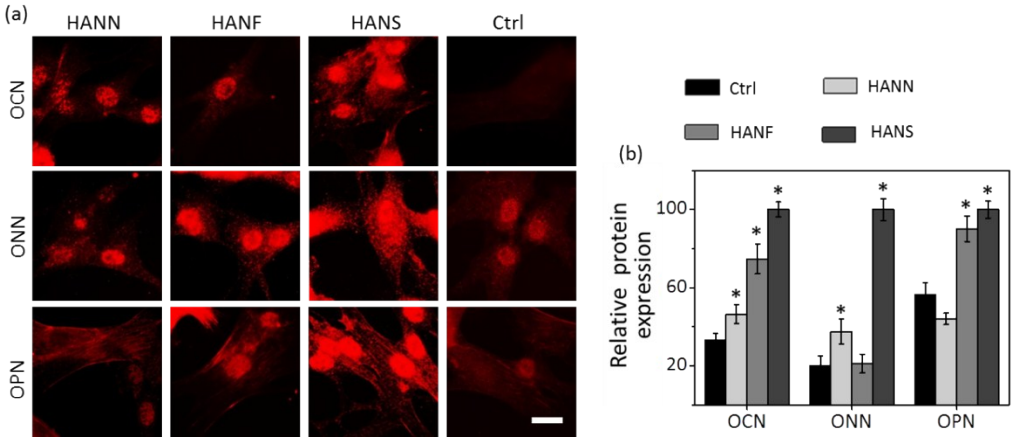

Fig. S8. Visualization (a) and quantification (b) of OCN, ONN and OPN markers with IF staining. Images were captured under the same condition for HANN, HANF, HANS, and control groups. Proteins

expression was up-regulated by Col-PAA/HA treatment, with more intense red fluorescence in IF images at the bottom line. Scale bar, 10 μm.

Supplemental Section 6: Fluorescent labelling of NPs

The NPs were chemically conjugated with a FITC label, followed by uptake process. Fluorescent microscope images (Fig. S9) of the labelled NPs reveal that all three kinds of NPs were readily labelled by FITC, and the fluorescent intensity for each kind of NPs seems almost the same.

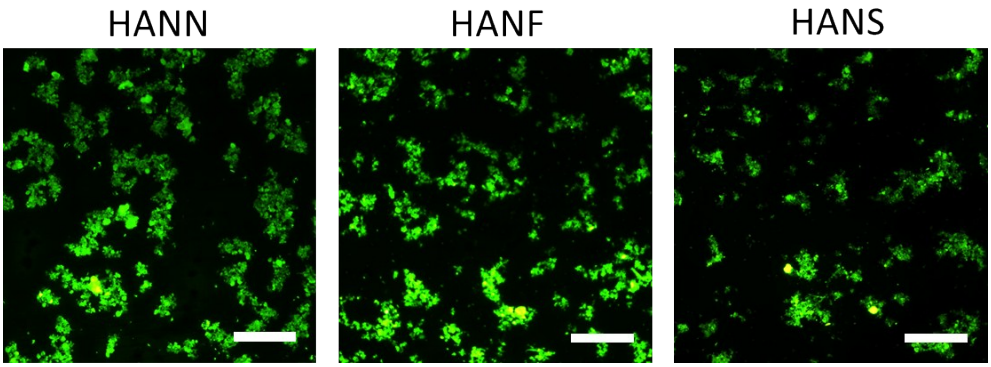

Fig. S9. Fluorescent microscope image of the HANN (left), HANF (middle), and HANS (right) labeled with FITC. The NPs can be readily conjugated with green fluorescence, and dispersed uniformly in H_2O. Scale bar, 100 μm.

Supplemental Section 7: IF evaluation for bone repair efficiency

IF images show that, blood vessels were developed in all groups (Fig. S10). It is notable that there were less residuals for HANS scaffold residuals, demonstrating a higher degradation rate.

In magnified IF images, abundant blood vessels and collagen fibers are visualized (Fig. S11). Note that the scaffold remains were non-specifically stained by both FITC and rhodamine label secondary IgG, giving a yellow fluorescence. Nuclei were counter-stained blue with DAPI. Blood vessels emerged in the spaces between scaffold residuals, indicating that neovascularization was in progress

simultaneously with osteogenesis. The abundance of tightly arrayed newly-formed collagen depicted the recovery level at the defect area.

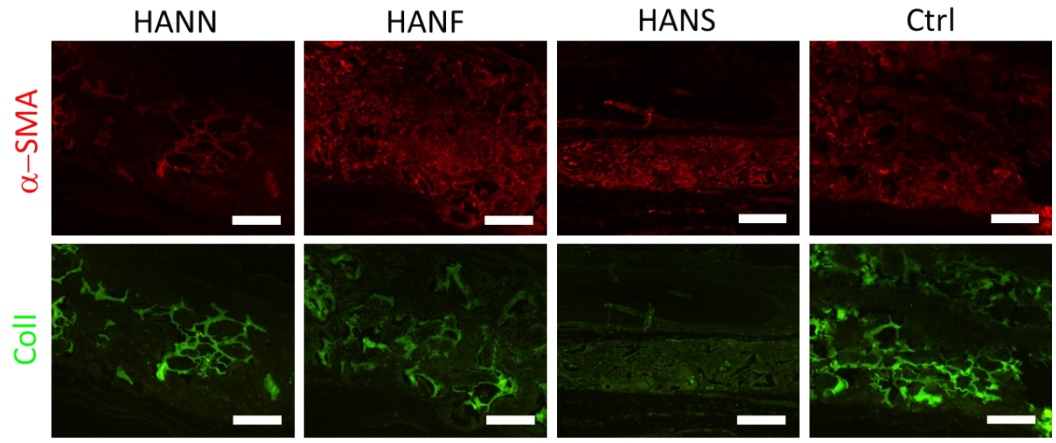

Fig. S10. IF staining of bone sections for α-SMA (upper) and Col I (bottom) in HANN, HANF, HANS, and NPs-free scaffolds 4 weeks after implantation. Scale bar: 100 μm.

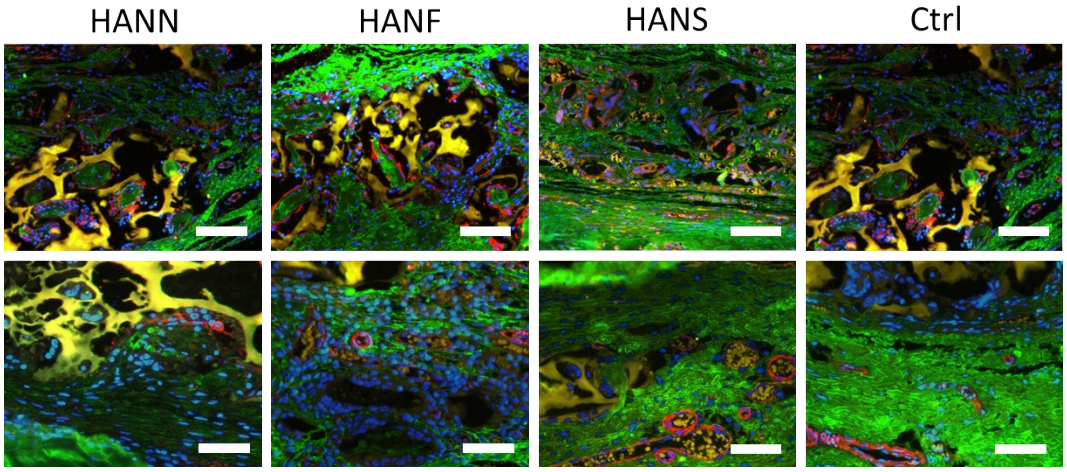

Fig. S11. IF staining for detailed evaluation of vascularized osteogenesis. Double-labelling of new regenerated collagen I (green) and blood vessels (red) for skull sections in HANN, HANF, HANS, and control group. Scale bars: top, 100 μm; bottom, 50 μm.

Supplemental Section 8: Methods

Cell culture. The rat mesenchymal stem cells (rMSCs) were purchased from Cyagen Biosciences Inc. and expanded in complete DMEM (10% FBS and pen/strep) at 37°C in 5% CO_2 prior to *in vitro* experiments.

NP treatment and cell proliferation. Cell viability and proliferation were determined using a cell counting kit (CCK-8, Sigma-Aldrich), following the manufacturer's instructions. NP-containing stock media were prepared with gamma irradiated HANN, HANF or HANS NPs to a concentration of 50 mg/mL in DMEM and test media (TM) prepared from the stocks to final NP concentrations of 0.02, 0.05 and 0.1 mg/ml. rMSCs were seeded in a 96-well plate at a density of 2,000 cells per well and incubated in DMEM for 24 h, after which the medium was replaced with TM. Cell viability was assessed at days 1 and 7 using the CCK-8 kit.

To determined the effect on cell proliferation of the individual components, rMSCs were cultured in DMEM supplemented with either pure bi-templates (Col-CS, Col-SA, and Col-PAA), as well as suspensions with the equivalent amount of pure HA (referred to as Col-CS&HA, Col-SA&HA, and Col-PAA&HA). Cell proliferation was assessed at days 1 and 7 days by CCK-8.

NPs internalization. To visualize the process of NP cellular uptake, the NPs were first conjugated with a green fluorescent label as described elsewhere.[3] Briefly, HANN, HANF, and HANS NPs were first coupled with an amino silane coupling agent, KH-550 (Sigma-Aldrich), and then conjugated with fluorescein isothiocyanate (FITC). The cells were incubated with 0.1 mg/ml FITC labeled NPs for 24 h, after which the intracellular lysosomes were stained red with lysotracker (Thermo Fisher, US). Cell nuclei were stained blue by Hoechst 33258 (Beyotime, China) and cell membranes labeled deep red with the Cellmask™ membrane probe (Thermo Fisher). Images were captured by CLSM (Olympus, Japan).

TEM imaging was also used to visualize intracellular location of the NPs.[4-5] The samples were prepared by first trypsinizing the treated cells and washing with phosphate buffer saline (PBS) before fixing with 5% (w/v) glutaraldehyde, followed by dehydrating through gradient ethanol and

embedding in epoxy resin. Ultrathin sections were prepared with an ultramicrotome, followed by electron staining in a 4% (w/v) uranyl acetate solution and TEM analysis, operating at 5 kV.

The quantity of NPs uptake was measured by flow cytometry. After 24 h incubation with FITC labeled NPs, the cells were trypsinized, washed with PBS, fixed with 4% paraformaldehyde (PFA), then permeabilized using 0.3% Triton X-100 and the nuclei stained with propidium iodide. The cells were subsequently sorted using a Cytomic™ FC 500 (Beckman, US).

Cell differentiation. The effect on osteogenic differentiation on rMCSs in the presence of the three types of NPs was assessed by *in vitro* experiments. Cells were seeded into a 48-well plate at a density of 4×10^4 cells/well. After 24 h, the medium was replaced with induction medium containing TM with HANN, HANF or HANS at 0.1 mg/ml final concentration. At days 3, 7, 14, the cells were harvested and lysed with a lysis buffer (Takara Biomedicals, Japan). Cellular ALP activity of each group was determined by LabAssay™ ALP kit (Wako, Japan) as described previously.[6] The total protein concentrations of the samples were determined using a Micro BCA Protein Assay Kit (Themo Fisher, USA) and the ALP activity normalized against total protein.

The expression of the osteogenic markers osteocalcin (OCN), osteonectin (ONN), and osteopontin (OPN) in rMSCs were assayed following NP treatment. MSCs were seeded into T25 culture flasks at a density of 10^5 cells /ml. At approximately 90% confluence, the media were replaced with HANN, HANF or HANS NPs containing TM at a final concentration of 0.1 mg/ml. After 14 days, total RNA was extracted by TRIzol (Thermo Fisher) and complementary DNA synthesized from 1 g of total RNA using SensiFast cDNA Synthesis Kit (Bioline, Australia). PCR primers were purchased from Sigma-Aldrich and primer sequences are listed in Supplementary Table 1. Gene expression analysis was performed on an ABI Prism 7500 Thermal Cycler (Applied Biosystems, Foster City, California, USA) using SYBR Green qPCR Master Mix (Thermo Fisher) reagent. Relative gene expression was normalized against the house keeping gene *GAPDH* and calculated using the ΔΔCt method. [7]

The cellular localization of osteogenesis-related proteins was visualized by immunofluorescence staining. After incubation in NP-containing medium for 3 weeks, the cells were washed and fixed with 4% PFA, permeabilized using 0.3% Triton X-100, then blocked with 5% (v/v) bovine serum albumin

(BSA). After blocking, the cells were incubated with rabbit anti-rat lgG for OCN, ONN, and OPN (all purchased from Santa Cruz Biotechnology, USA) overnight at 4°C and labeled with rhodamines-conjugated goat anti-rabbit secondary antibodies. FITC-conjugated phalloidin was used to stain F-actin and 4,6-diamidino-2-phenylindole (DAPI, Beyotime, China) for cell nuclei. Images were captured with a Nikon Eclipse Ti fluorescence microscope (Nikon, Japan) and the relative fluorescent intensities quantified using ImageJ.

Activation of autophagy. Autophagy activation in MSCs was assessed following stimulation with TM. Light chain 3 (LC3) is a key marker of autophagy and its expression used as an indication for the degree of autophagy activation. MSCs were incubated with TM at final concentrations at 0.1 mg/ml for 1 and 3 days and total RNA harvested with TRIzol. The mRNA expression of LC3A and LC3B was assayed by RT-qPCR as described above and primers sequences are listed in Supplementary Table S1.

The cellular expression and localization of LC3A/B was visualized with IF staining. Cells were seeded onto 12 mm coverslips at a density of 10^4 cells per coverslip and allowed to settle for 24 h, after which the medium was replaced with TM and incubated for a further 3 days. The cells were fixed in 4% PFA and stained with a rabbit monoclonal LC3A/B antibody at 1:100 dilution (Cell Signaling Technology) followed by Alexa Fluor 488 Conjugate anti-rabbit IgG secondary antibody (1:500; Cell Signaling Technology) and DAPI and Rhodamine-conjugated phalloidin. Images were captured on a Leica SP5 confocal microscope and the relative fluorescent intensities quantified using ImageJ.

Statistical analysis. All data were expressed as mean ± s.d. The unpaired, two-sided Student t-test was used for variance analysis between groups. *$p < 0.05$ was considered significant, and *$p < 0.01$ was considered highly significant.

Table S1. Primer sequences for P2X7, P2X4, OCN, Runx-2, VEGF, IDH3 genes.

Primer No.	Primer name	Primer sequences (5'-3')	length(bp)
NM_017008.4	R-GAPDH-S	TTCCTACCCCCAATGTATCCG	281
	R-GAPDH-A	CATGAGGTCCACCACCCTGTT	
NM_013414.1	R-OCN-S	AGGGCAGTAAGGTGGTGAATAGA	146
	R-OCN -A	GAAGCCAATGTGGTCCGCTA	
M14656.1	R-OPN-S	GATGAACAGTATCCCGATGCC	217
	R-OPN-A	CCCTCTGCTTATACTCCTTGGAC	
NM_012656.1	R-ONN-S	GAGAGAGATGAGGGCAACAACC	356
	R-ONN-A	TTGATGTCCTGCTCCTTGATGC	
NM_001278483.1	R-Runx2-S	CAGTATGAGAGTAGGTGTCCCGC	152
	R-Runx2-A	AAGAGGGGTAAGACTGGTCATAGG	
NM_199500.2	R-LC3A-S	TGTCCTGGATAAGACCAAGTTTC	170
	R-LC3A-A	CCTGTTCATAGATGTCAGCGAT	
NM_022867.2	R-LC3B-S	AGAGCGATACAAGGGTGAGAAG	134
	R-LC3B-A	AGAAGGCTTGGTTAGCATTGAG	
NM_130405.1	R-P62-S	TGGACCACAAGGAAATACAATCA	98
	R-P62-A	CCTCCTTGGCTTTGTCTCTCATC	

References

1. Liou, S. C.; Chen, S. Y.; Liu, D. M. Manipulation of Nanoneedle and Nanosphere Apatite/Poly(Acrylic Acid) Nanocomposites. *J. Biomed. Mater. Res. B Appl. Biomater.* **2005,** *73*, 117-122.
2. Du, Y.; Liu, H.; Shuang, J.; Wang, J.; Ma, J.; Zhang, S. Microsphere-Based Selective Laser Sintering for Building Macroporous Bone Scaffolds with Controlled Microstructure and Excellent Biocompatibility. *Colloids Surf. B Biointerfaces* **2015,** *135*, 81-89.
3. Ojea-Jimenez, I.; Garcia-Fernandez, L.; Lorenzo, J.; Puntes, V. F. Facile Preparation of Cationic Gold Nanoparticle-Bioconjugates for Cell Penetration and Nuclear Targeting. *ACS Nano* **2012,** *6*, 7692-7702.

4. Brayner, R.; Ferrari-Iliou, R.; Brivois, N.; Djediat, S.; Benedetti, M. F.; Fievet, F. Toxicological Impact Studies Based on Escherichia Coli Bacteria in Ultrafine ZnO Nanoparticles Colloidal Medium. *Nano Lett.* **2006,** *6*, 866-870.
5. Xia, L.; Lin, K.; Jiang, X.; Fang, B.; Xu, Y.; Liu, J.; Zeng, D.; Zhang, M.; Zhang, X.; Chang, J.; Zhang, Z. Effect of Nano-Structured Bioceramic Surface on Osteogenic Differentiation of Adipose Derived Stem Cells. *Biomaterials* **2014,** *35*, 8514-8527.
6. Nikukar, H.; Reid, S.; Tsimbouri, P. M.; Riehle, M. O.; Curtis, A. S.; Dalby, M. J. Osteogenesis of Mesenchymal Stem Cells by Nanoscale Mechanotransduction. *ACS Nano* **2013,** *7*, 2758-2767.
7. Shim, W.; Paik, M. J.; Nguyen, D. T.; Lee, J. K.; Lee, Y.; Kim, J. H.; Shin, E. H.; Kang, J. S.; Jung, H. S.; Choi, S.; Park, S.; Shim, J. S.; Lee, G. Analysis of Changes in Gene Expression and Metabolic Profiles Induced by Silica-Coated Magnetic Nanoparticles. *ACS Nano* **2012,** *6*, 7665-7680.